Available online at www.sciencedirect.com
ScienceDirect
Ceramics International 36 (2010) 141–149
CERAMICS INTERNATIONAL
www.elsevier.com/locate/ceramint

Influence of critical plasma spraying parameter (CPSP) on plasma sprayed Alumina–Titania composite coatings

S. Yugeswaran [a], V. Selvarajan [a,*], M. Vijay [a], P.V. Ananthapadmanabhan [b], K.P. Sreekumar [b]

[a] *Plasma Physics Laboratory, Department of Physics, Bharathiar University, Coimbatore 641046, India*
[b] *Laser and Plasma Technology Division, Bhabha Atomic Research Centre, Mumbai 400085, India*

Received 10 September 2008; received in revised form 27 April 2009; accepted 6 July 2009
Available online 11 August 2009

Abstract

Plasma sprayed ceramic coatings are successfully used in many industrial applications, where high wear and corrosion resistance with thermal insulation are required. Critical plasma spraying parameter (CPSP) is a key factor to control the quality of coatings. In this study, Alumina–Titania composite coatings in different compositions (Alumina–3 wt.% Titania, Alumina–13 wt.% Titania and Alumina–40 wt.% Titania) were prepared by 40 kW atmospheric plasma spray torch at three different CPSP conditions (833.33, 1000 and 1166.66) and their influence on coatings and plasma jet temperature were studied. The phase, microstructure, sliding and erosive wear rates, microhardness and porosity of the different Alumina–Titania composite coatings was investigated and correlated to CPSP conditions. The result shows that increasing CPSP increases the hardness and anti wear behavior of Alumina–Titania composite coatings except Alumina–40 wt% Titania coating.

Keywords: B. Porosity; B. Composites; C. Wear resistance; D. Al_2O_3; D. TiO_2

1. Introduction

Plasma spraying is a thermal spray process in which finely divided metallic and non-metallic materials are deposited in a molten or semi-molten state on a prepared substrate. Due to high flame temperature, a satisfactory melting state can be achieved, which is beneficial for formation of dense coatings with a variety of properties required for industrial applications. Ceramic coatings produced by atmospheric plasma spraying techniques are increasingly and widely used for a wide range of industrial applications to provide wear and erosion resistance, corrosion protection and thermal insulation. For example, plasma sprayed Al_2O_3/TiO_2 coatings have been widely used as wear resistance coatings in textile, machinery, and printing industries [1–7]. In plasma spraying, feedstock powder is melted and accelerated to high velocities (100 m/s), impinging upon the substrate, and rapidly solidifying (10^5 to 10^6 k/s) to form a ''splat'' (a flattened particle) [8]. The deposit develops by successive impingement and inter-bonding among the splats. The deposit microstructure is strongly dependent on processing conditions, spray parameters and feedstock materials. Particularly plasma spraying parameters such as input power, plasma forming and secondary gas flow rate, standoff distance, transverse speed, carrier gas flow and powder feed rates, angle and location of powder injection-port and spraying angle directly or indirectly influence the microstructure and physical properties of the coating [9,10]. However, plasma torch input power and plasma forming gas flow rate are main parameters to control the nature of coatings. Some researchers have combine these two parameters and introduced the critical plasma spraying parameter (CPSP) for coating optimization. The critical plasma spraying parameter (CPSP) is defined as [4,5]

$$\text{CPSP} = \frac{\text{input power(kW)}}{\text{primary gas flow rate(lpm)}} \quad (1)$$

As shown in Eq. (1), CPSP is expressed as the plasma output power in the numerator and the primary gas (Ar) flow rate in the denominator. It is well known that when the plasma output power is increased, the particle temperature increases due to increasing plasma jet temperature because it is very sensitive to CPSP. The decrease in the argon flow rate, which leads to an increase in the powder in-flight time, has a similar effect on the

* Corresponding author. Tel.: +91 422 2426576; fax: +91 422 2422387.
E-mail address: vselvrjn47@rediffmail.com (V. Selvarajan).

0272-8842/$36.00
doi:10.1016/j.ceramint.2009.07.012

particle temperature as the increase in the plasma output power. So CPSP can alter the coating microstructure and properties, but is not the only way to adjust the coating microstructure and properties. In this study, we have studied the influence of CPSP on plasma jet temperature, microstructure, phase composition, erosive wear rate, sliding wear rate, hardness and porosity (%) of the plasma sprayed three different types of Alumina–Titania composites coatings.

2. Experimental procedure

2.1. Substrate preparation

Mild steel substrate (AISI 4626) of composition (0.25%C, 0.7%Mn, 0.25% Si, and 0.05%S) was employed throughout for coating deposition. The dimensions of the mild steel specimens used for microstructure investigation are 50 mm × 20 mm × 2 mm; for erosive wear is 50 mm × 50 mm × 2 mm; and for sliding wear a pin 12 mm in diameter and 50 mm long. The required dimensions of the substrates were prepared by using abrasive cutting machine (Metco). Before coating, grid blasting of the steel samples was carried out using a grid blasting machine with 75–125 μm size sand at an air pressure of about 50 psi, at a distance of about ∼150 mm. The resulting average surface roughness was about 10 μm Ra. Subsequent to grid blasting, the samples were cleaned with forced air and acetone.

2.2. Coating preparation

Three compositions of Alumina–Titania were used for coatings. Coatings were prepared by 40 kW atmospheric plasma spray torch (Ion Arc technologies, India). The Alumina–Titania composite was prepared by blending and fusing (M/s Carborundum Universal Ltd., India). The chemical composition and powder size used as base materials are given in Table 1. The parameters of the plasma spraying conditions are summarized in Table 2. Normally argon gas is used for plasma spraying due to its nature for operation and low cost. Addition of small amount of nitrogen with argon gas enhances the specific enthalpy and thermal conductivity of the plasma jet. The addition of nitrogen gas also increases the average plasma jet temperature, jet length and strongly influences the in-flight particle temperature.

For the microscopic observation and the microhardness measurements, the coated samples were cut for cross-section by using diamond wheel with a cutting speed of 20 μm/s and mounted metallographically before grinding and polishing. The samples were grounded with standard SiC grinding papers starting from 400 grid and finishing off with 1200 grid under constant load (5 N) and running duration (2 min). The samples were then lightly polished using 1 μm diamond paste. Microhardness values of the specimens were taken from the cross-section of the polished samples at a load of 2 N using LEITZ microhardness tester. The average values (ten points) of the measured microhardness are reported. The microstructure of the coatings was characterized by scanning electron microscopy (SEM). The phase composition of the coating was examined by X-ray diffraction (XRD) with nickel filtered Cu Kα (λ: 1.54056 Å) radiation on a Philips analytical diffractometer.

Table 1
Details of used powders.

S. no.	Composition of Alumina–Titania blends (wt%)	Particle size (μm)	True density (kg m^{-3})
1	97%Alumina–3% Titania	10–40	3950
2	87%Alumina–13% Titania	10–40	4050
3	60%Alumina–40% Titania	10–40	4120

Table 2
Plasma spraying conditions.

Critical Plasma Spray Parameter	833.33; 1000; 1166.66
Primary gas (Ar) flow rate	30 lpm
Secondary gas (N_2) flow rate	5 lpm
Powder carrier gas (Ar) flow rate	10 lpm
Powder flow rate	10 gpm
Nozzle diameter	8 mm
Spray distance	100 mm
Powder injection	Radial; 5 mm before the nozzle exit
Internal diameter of the injector	3 mm
Plasma gas injection	Vortex injection

2.3. Plasma jet temperature

The excitation temperature of plasma jet is generally called plasma jet temperature. The plasma jet temperature along the line of sight at nozzle exit can be determined by the atomic Boltzmann plot method from the following equation [11,12]:

$$\log\left(\frac{I\lambda}{g_k A_k}\right) = C - \left(\frac{625E_k}{T}\right) \quad (2)$$

or

$$T = \frac{-625}{\text{slope value}} \quad (3)$$

A plot between $\log(I\lambda/g_kA_k)$ and E_k yields a straight line by best fit method. The inverse of the slope of the line gives the excitation temperature of the plasma jet along the line of sight, where I is the intensity and λ is the wave length of the line; C is the intercept on the ordinate axis; A_k is transition probability; E_k and g_k are the excitation energy and statistical weight of atomic state k, respectively.

The emission spectra of plasma jet were recorded by the monochromator (Thermo Oriel, 1/4 M) based diagnostic arrangements (Fig. 1) along with a photomultiplier tube, power supplies, oscilloscope, *X–T* recorder and a computer for running the monoutility program and optical fiber with *xyz* positioner for collecting radiation from the plasma jet. The values of intensities were calculated from the spectrum and g_k, A_k, and E_k values of corresponding lines were taken from literature [13]. Using a software log $(I\lambda/g_kA_k)$ vs. E_k was plotted. The slope was obtained from the straight line of the best fit and the correlation coefficient was more than 0.85 to give the best fit for random points.

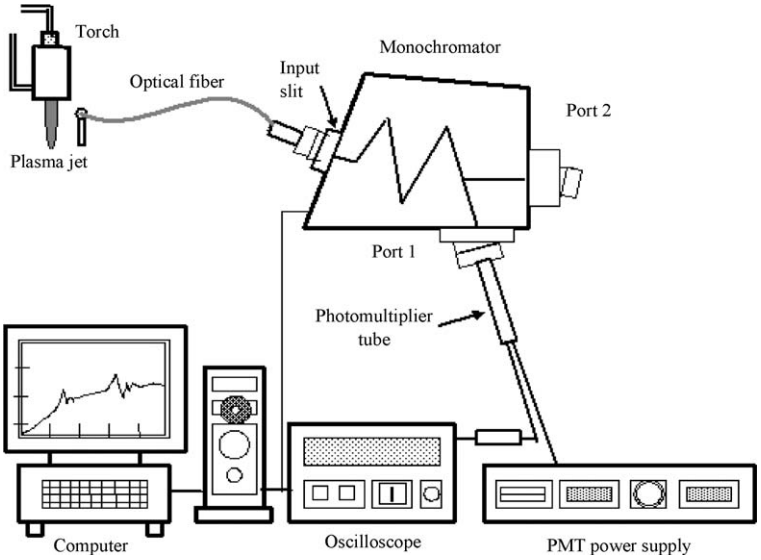

Fig. 1. Diagnostic arrangement for temperature measurement.

2.4. Sliding wear

The sliding wear study of plasma sprayed Alumina–Titania composites was carried out using pin-on-disk sliding wear machine (model TR–20 of Ducom, India). Tests were conducted on plasma sprayed 12 mm (diameter) cylindrical pins. These pins were polished using 1200 grit polishing paper. Sliding wear test samples were pressed against the disc with a specified force of 49.05 N. The number of rotations of the disc was preset to correspond a sliding distance of 3.4 km with a sliding velocity of 1.884 m/s for a duration of 30 min and the machine was then allowed to run continuously without interruption. The sliding wear tests of specimens were conducted against polished stainless steel (EN-31) disc having 100 mm diameter and 8 mm thickness. The specific wear rate is defined as the wear volume normalized by the normal load and the sliding distance. The following relationship was used to estimate the specific wear rate, W_s of samples [14,15]:

$$W_s = \frac{V}{DL} \tag{4}$$

where V is the volume loss, D is the sliding distance and L is normal load applied on the specimen. The volume loss $V = m/\rho$, where ρ is the density of the material, m is the mass loss. The mass loss (m) was measured after each set of run and volume loss (V) was estimated by using density (ρ) of sample. The coefficient of friction (μ) between the composite specimen and steel plate (EN-31) was directly obtained from the equipment using a transducer attached with test equipment and was recorded using computer interface. The steel disc was cleaned and polished every time to remove debris or remnants of transfer layer, etc. before fixing a new specimen for sliding test. After completion of specified sliding distance the test samples were cleaned using a soft brush to remove the worn particles before weighing the samples.

2.5. Erosive wear

A sand blasting machine (Fig. 2) as used to study erosive wear behavior of the coating materials. The sample (50 mm × 20 mm × 2 mm) was fixed in a substrate holder which could be moved in two ways. By horizontal movement, distance between the blast gun and the sample could be adjusted; while by rotation along the vertical axis, angle of impact could be changed. The erodent through hopper and blast gun was impinged on the sample with preset angle. Air pressure could be adjusted with a regulator so as to enable pressure of the erodent impinging on the sample. The erosion test sample was subjected to erosion for a fixed period of time (1 min), cleaned with acetone, dried and weighed. The weight loss on the test specimen during each exposure was determined.

The dimensionless erosion rate (W_e) was then estimated as a ratio of an average weight loss of tested coating surface overlay and weight of erodent striking the surface of specimen, has been chosen as a criterion for the estimation of erosive wear [16]:

$$W_e = \frac{W_l}{W_t} \tag{5}$$

where W_l is the weight loss of the coating surface and W_t is the total weight of the striking erodent particles. This test was

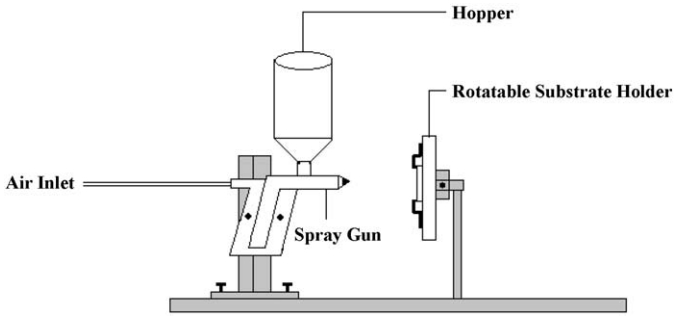

Fig. 2. Schematic drawing of erosive wear testing sand blasting machine.

Table 3
Operating parameters.

Erodent	Silica sand (particle size: 90–120 μm)
Flow rate of sand	500 g/min
Impact angle	30, 60 and 90°
Air pressure	45 psi
Nozzle diameter	3 mm
Distance (between the blast gun and the sample holder)	10 cm

repeated until W_e attained a steady-state value. Erosion tests were carried out with three different impact angles. The operating parameters are given in Table 3.

2.6. Porosity level (%)

The porosity level of the coatings can be calculated by the Archimedes' principle. The non-connected porosity level of each coating was evaluated by Eq. (6):

$$\text{porosity}(\%) = 100 - \frac{\text{coating density}}{\text{bulk density}} \times 100 \quad (6)$$

For this study, self-standing samples were prepared with a thickness around 300 μm. The density of the coatings was measured by water immersion method [17,18]:

$$\text{coating density} = \frac{D}{W - S} \quad (7)$$

where D, W and S are dry, saturated and suspended weights of the coating material, respectively.

3. Results and discussion

3.1. CPSP effect on plasma jet temperature

Fig. 3 shows the emission spectra of argon plasma jet at 400–450 nm wavelength regions. Ten distinguishable Ar–I lines (namely 404.44, 415.80, 418.18, 419.10, 420.06, 425.93, 427.91, 430.01, 433.35 and 451.07 nm) were observed. The intensity of these lines is used to calculate the temperature of plasma by atomic Boltzmann plot method. Fig. 4 shows the plasma jet temperature as a function of CPSP. The temperature of the plasma jet gradually increases with increasing CPSP.

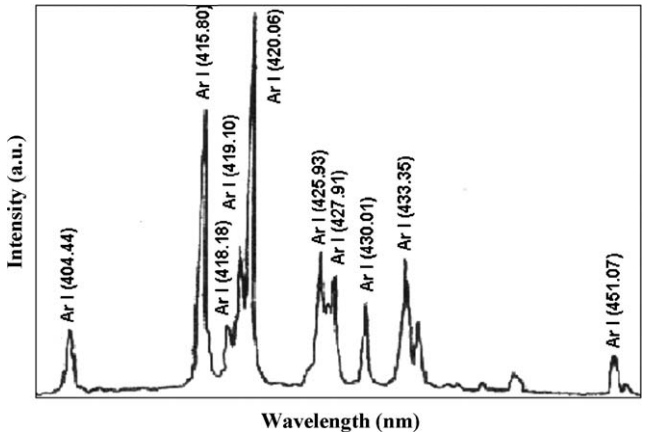

Fig. 3. Emission spectra of the argon plasma jet.

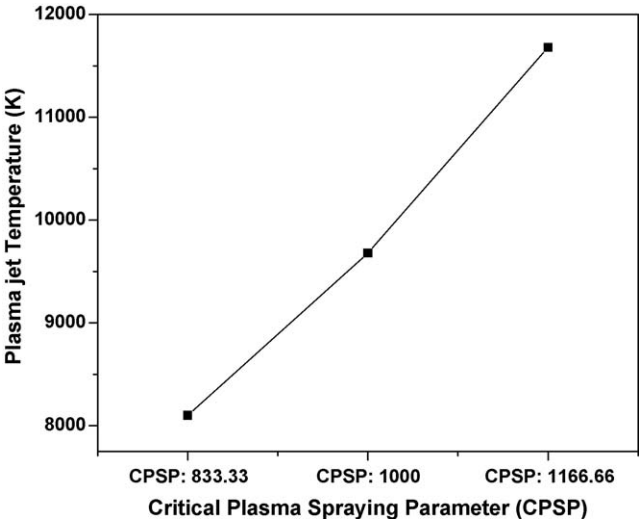

Fig. 4. Plasma jet temperature at the nozzle exit.

Fig. 4 shows the plasma jet temperature as a function of CPSP conditions. While increasing the CPSP from 833.33 to 1166.66, the plasma jet temperature rises from 8100 to 11680 K. The increasing CPSP is inclusive of increase in torch input power. In higher plasma temperature, the plasma jet velocity and heat transfer rate from plasma to particles also increases.

3.2. CPSP effect on phase and microstructure

Fig. 5 shows the XRD patterns of the Alumina–3% Titania coatings performed at various CPSP conditions (CPSP 833.33, 1000 and 1166.66), which reveal a similar phase composition in

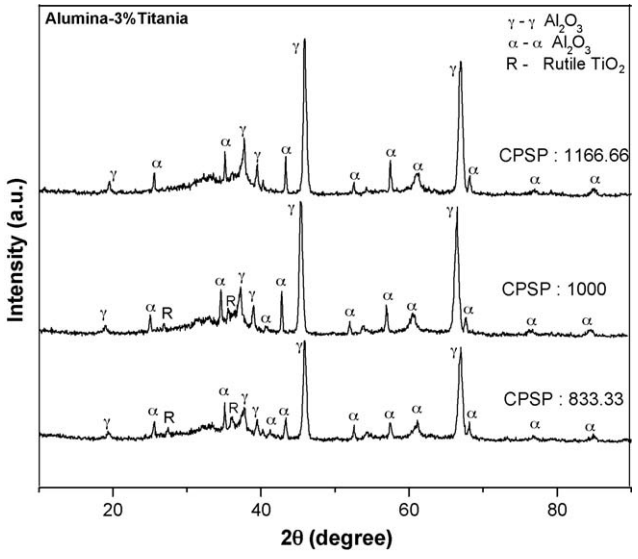

Fig. 5. XRD pattern of plasma sprayed Alumina–3% Titania composite coating.

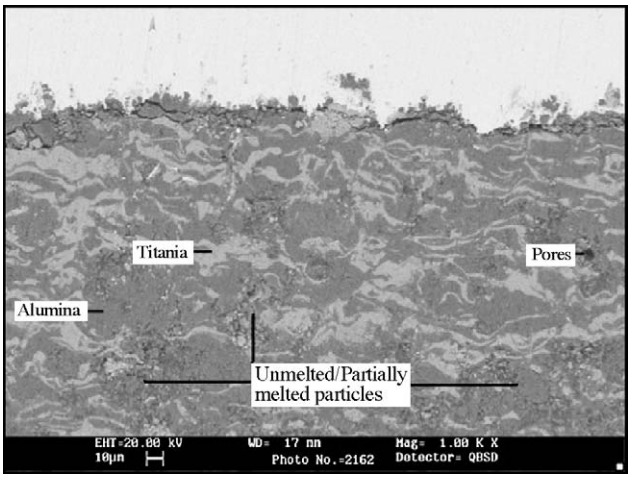

Fig. 6. SEM image of Alumina–13% Titania composite coating at CPSP 1166.66.

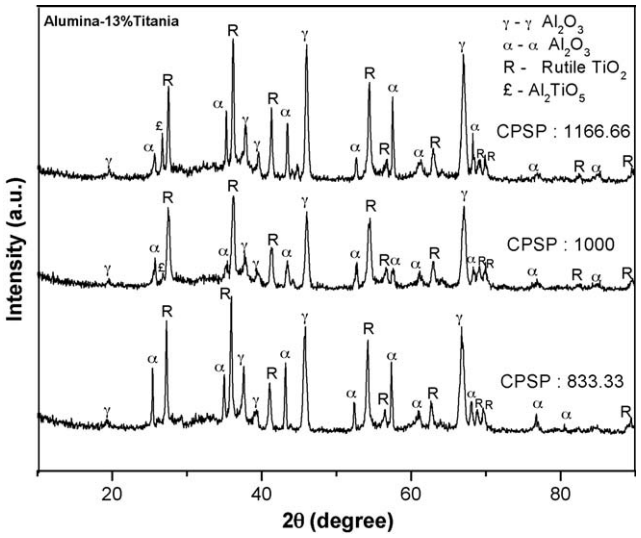

Fig. 7. XRD pattern of plasma sprayed Alumina–13% Titania composite coating.

all cases. Different phases of alumina exist in these plasma sprayed coatings: γ-Al_2O_3 is the predominant phase and α-Al_2O_3 is the minority phase and diffraction lines of Rutile–Titania could also be identified. The partial transformation of α-Al_2O_3 to γ-Al_2O_3 in the deposited coatings is due to the plasma spray conditions and cooling process. The existence of γ-Al_2O_3 clearly indicates that the alumina in Alumina–3% Titania coatings is rapidly solidified process. In spite of the similarity among the various CPSP conditions of coatings, difference is obvious too when the intensities of XRD patterns are examined carefully.

The crystallinity of each phase increases while increasing CPSP, which results to enhance microstructure of the coatings. Fig. 6 shows the SEM image of plasma sprayed Alumina–13% Titania composite coating at CPSP 1166.66. The image clearly shows the coating surface consists of pores, voids and unmelted/partially melted particles.

Fig. 7 shows the XRD patterns of the Alumina–13% Titania composite coatings performed at various CPSP conditions (CPSP 833.33, CPSP 1000 and CPSP 1166.66), which reveal Rutile–Titania as the major phase compared to γ-Al_2O_3 and α-Al_2O_3. In addition, the presence of metastable Al_2TiO_5 phase was identified at CPSP 1000 and the formation of Al_2TiO_5 phase increases while increasing CPSP (Fig. 8). The Al_2TiO_5 phases have formed as a result of reaction between TiO_2 and Al_2O_3 and the formation of Al_2TiO_5 phase depends on solubility of TiO_2 in Al_2O_3 structure and the process temperatures [19].

It is known that the addition of TiO_2 to the Al_2O_3 coating is to reduce the melting temperature of the oxide, thereby

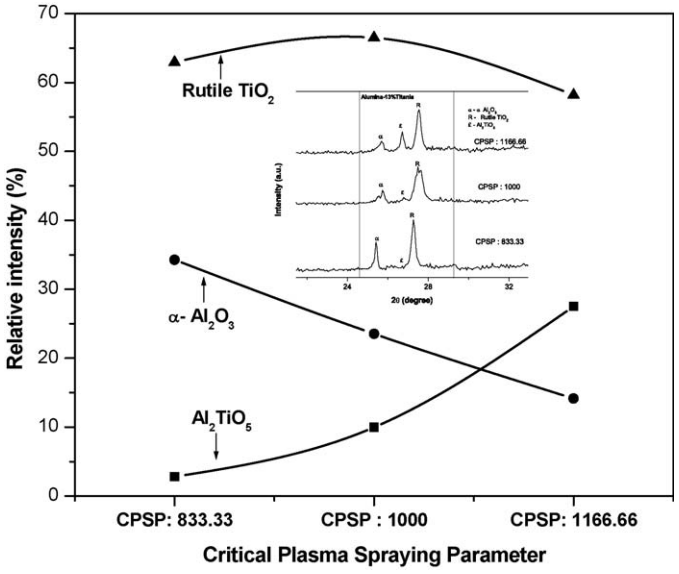

Fig. 8. Effect of CPSP on relative intensity of plasma sprayed Alumina–13% Titania composite coating.

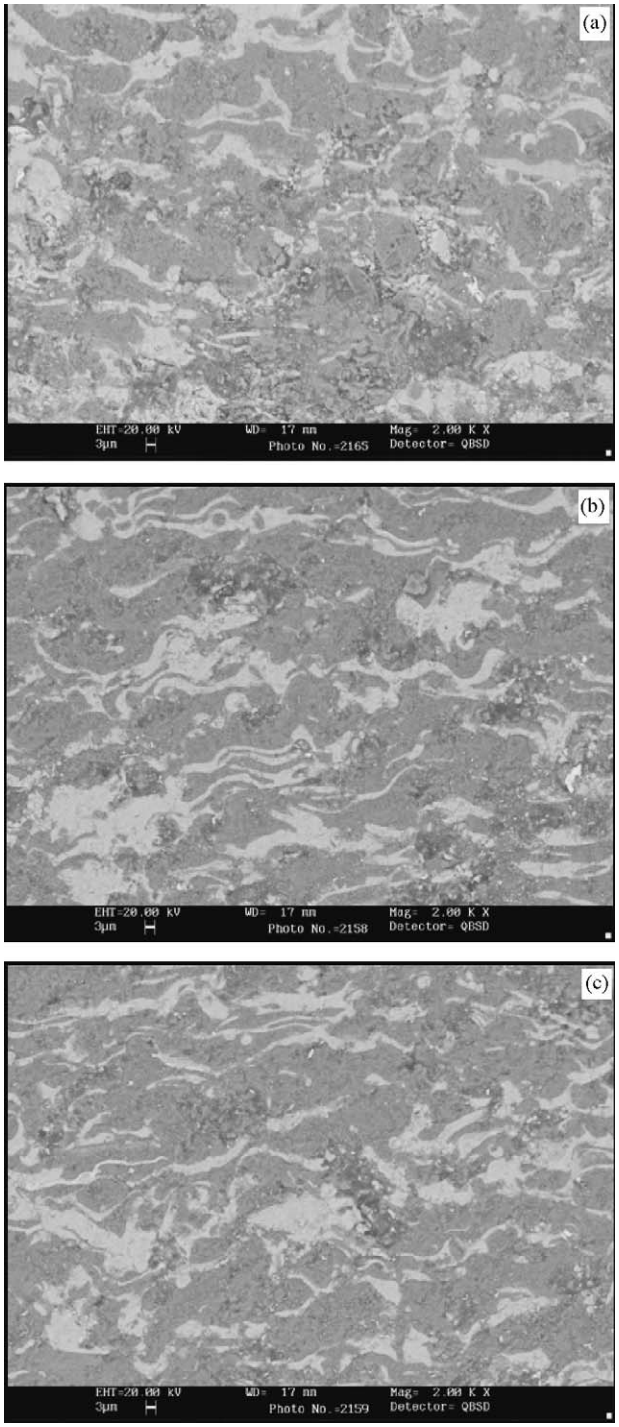

Fig. 9. SEM image of plasma sprayed Alumina–13% Titania composite coating at (a) CPSP 833.33, (b) CPSP 1000 and (c) CPSP 166.66.

producing less porous and better performance coatings than pure Al_2O_3 coatings [2,20]. The decreased melting temperature is due to the fact that TiO_2 has a lower melting temperature (1854 °C) than Al_2O_3 (2040 °C) and its ability to form a liquid solution with Al_2O_3 [21]. The degree of melting of the powder particle during plasma spray, however, also depends on the thermal conductivity of the particle itself.

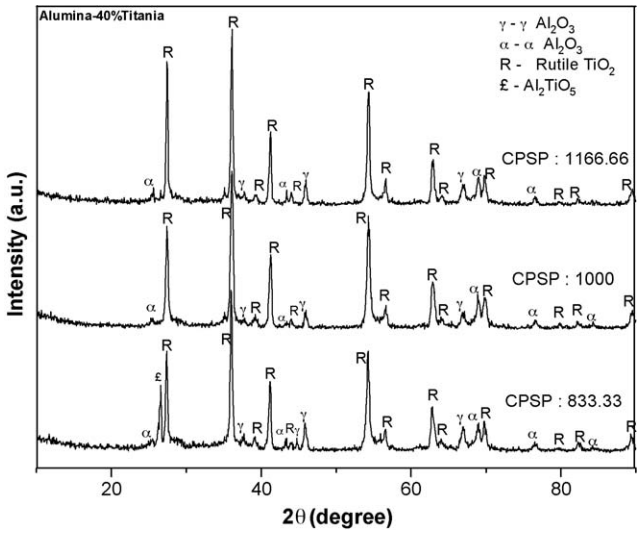

Fig. 10. XRD pattern of plasma sprayed Alumina–40% Titania composite coating.

Fig. 9 shows the SEM image of plasma sprayed Alumina–13% Titania composite coating at different CPSP conditions. It is clearly seen from the figure that the unmelted or partially melted particles are present in the coating and the porosity exists in all the coatings. Although colour of the phases is not distinguished in all the coatings, white regions in the coatings are attributed to Titania while grey ones to Alumina. Fig. 10 shows the XRD patterns of the Alumina–40% Titania composite coatings performed at various CPSP conditions (CPSP 833.33, 1000 and 1166.66), which reveal Rutile–Titania as the predominant phase compared to γ-Al_2O_3 and α-Al_2O_3. In addition, the presence of metastable Al_2TiO_5 phase was also identified at CPSP 833.33. The intensity of γ-Al_2O_3 and α-Al_2O_3 peaks are weak in Alumina–40% Titania coatings at all CPSP conditions.

The phase formation of $Al_2O_3 + TiO_2$ coatings is influenced by heat transferred from plasma to particles, quenching rate of molten particles and powder shape and size distribution. In all the coatings γ-Al_2O_3 and α-Al_2O_3 are found. The presence of α-Al_2O_3 phase is due to incomplete melting of larger particles. The partially melted particles form coatings in α-Al_2O_3 structure due to the core of the same in α-Al_2O_3 phase.

The slow quenching rate is not possible in the above said spray conditions because plasma torch is not concentrated on the coating for a long time. γ-Al_2O_3 phase is due to complete melting of the particles and the high rate of heat removal from the deposit. On the basis of nuclear kinetics γ-Al_2O_3 is more easily nucleated from the melt than α-Al_2O_3 because of the lower interfacial energy between the γ-Al_2O_3 structure and the liquid [22]. Alumina and Alumina–Titania systems have a high tendency to produce different phases and crystallographic structure changes according to the cooling process, deposition techniques, material spray condition etc. The structure changes and its consequence on the deposited layer properties have been studied in this work. Fig. 11 shows the surface morphology of plasma sprayed Alumina–40% Titania composite coating at

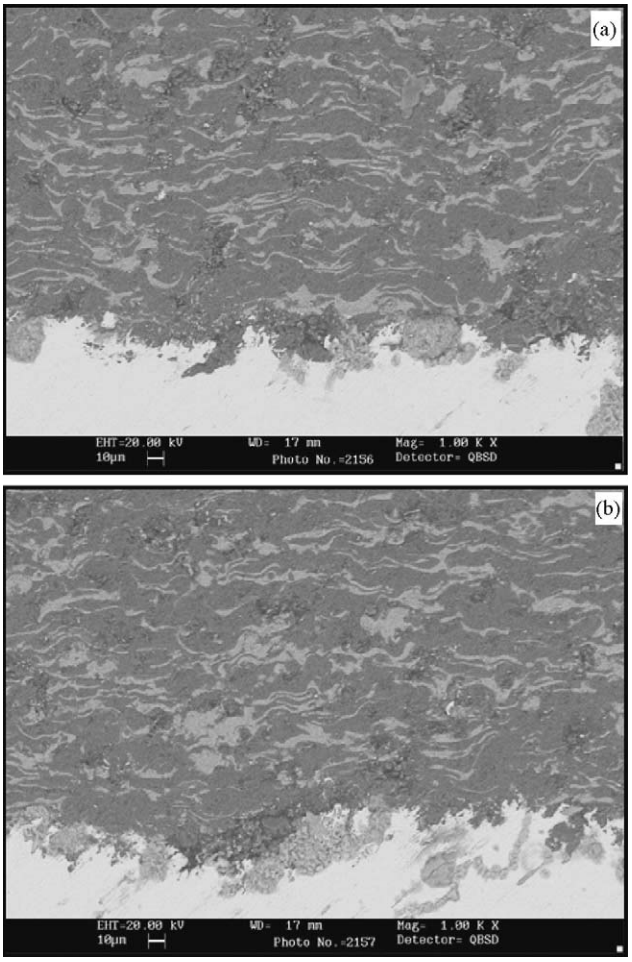

Fig. 11. SEM of Alumina–40% Titania composite coating: (a) CPSP 833.33 and (b) CPSP 1166.66.

CPSP 833.33 and 1166.66. The coating at CPSP 166.66 clearly shows the higher porosity than that of CPSP 833.33.

3.3. CPSP effect on microhardness

Fig. 12 shows the microhardness of the plasma sprayed on three different compositions of Alumina–Titania composite coatings as a function of CPSP conditions. Except Alumina–40% Titania coating the microhardness value increases with increasing CPSP. Generally increasing CPSP gives dense and porosity less coatings due to higher degree of melting and high impact velocity of molten particles. In principle, the microhardness values of Alumina–Titania composite coatings depend on their composition. Microhardness tends to decrease with Titania addition [24–26]. In this study, Alumina–3% Titania composite coating gives maximum hardness value at CPSP 1166.66. At the same time very low hardness value is obtained for Alumina–40% Titania composite coating at CPSP 1166.66.

3.4. CPSP effect on porosity level (%)

Fig. 13 shows the porosity level (%) of the plasma sprayed on three different compositions of Alumina–Titania composite

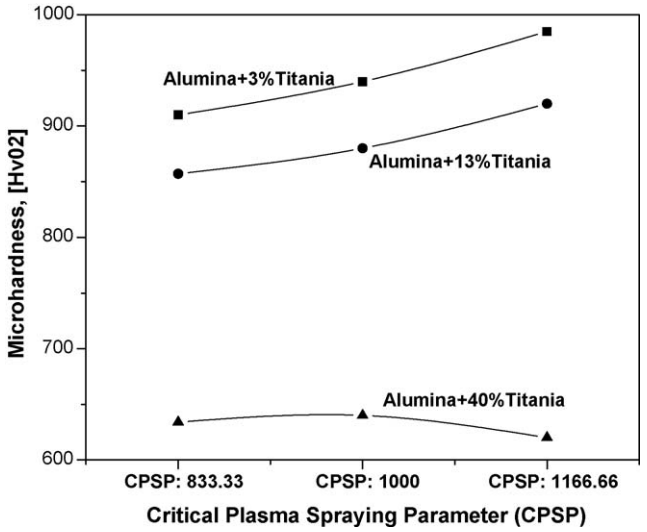

Fig. 12. Effect of CPSP on the microhardness of the plasma sprayed Alumina–Titania composite coatings.

coatings as a function of CPSP conditions. In Alumina–3% Titania and Alumina–13% Titania composite, the porosity level decreases with increasing CPSP. The coatings are formed by the piling of melted droplets. A higher particle velocity before impact may be expected to give better spreading. Complete melting of the particles and higher velocity will yield lesser porosity in the coating. Hence increasing CPSP gives low porosity coatings. However porosity of Alumina–40% Titania composite coating increased with increasing CPSP conditions. The lowest porosity was obtained for Alumina–13% Titania composite at CPSP 1166.66.

3.5. CSPS effect on sliding wear rate

Fig. 14 shows the sliding wear behavior of plasma sprayed different compositions of Alumina–Titania composite compo-

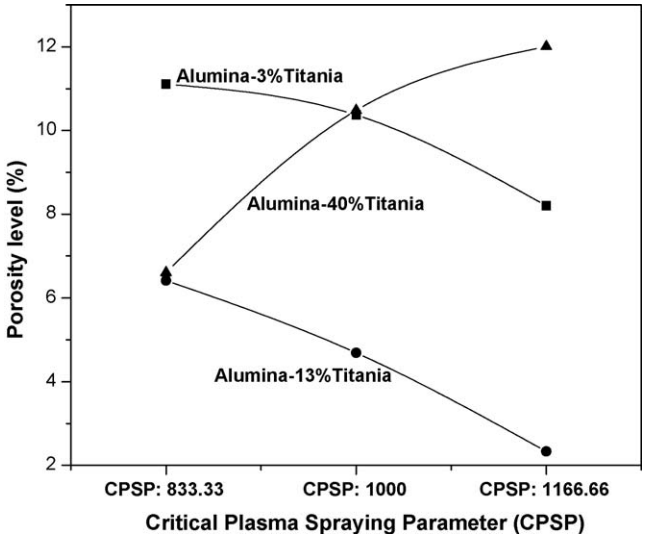

Fig. 13. Effect of CPSP on the porosity level (%) of the plasma sprayed Alumina–Titania composite coatings.

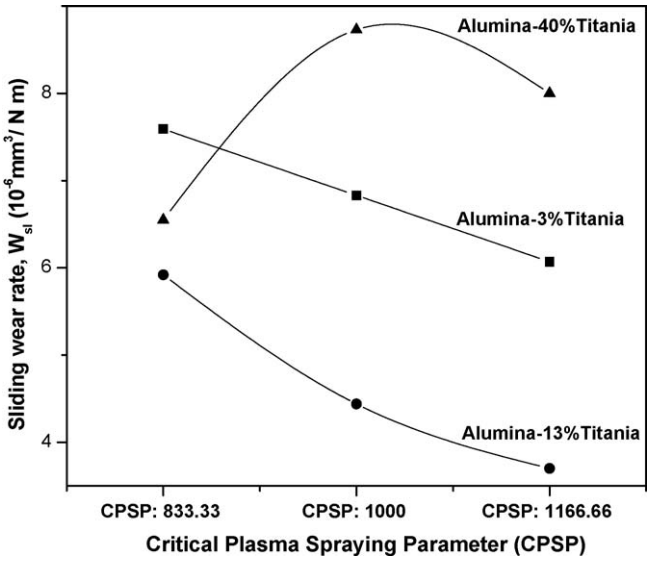

Fig. 14. Effect of CPSP on the Sliding wear rate of the plasma sprayed Alumina–Titania composite coatings.

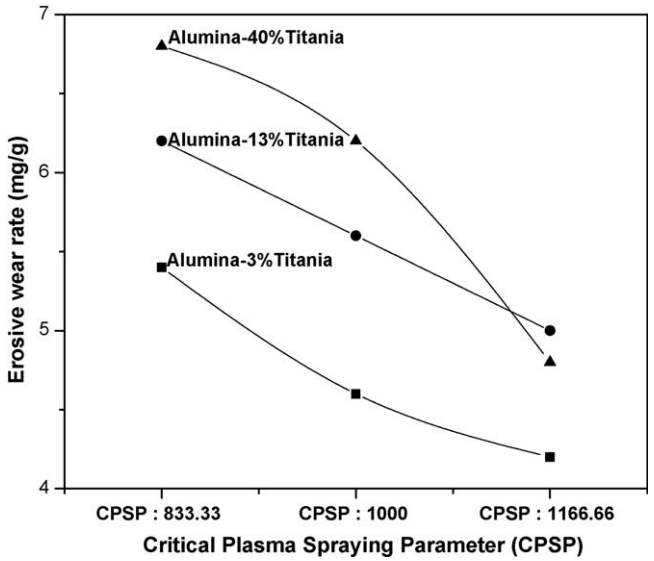

Fig. 16. Effect of CPSP on the erosive wear rate of the plasma sprayed Alumina–Titania composite coatings.

site coating at different CPSP conditions. Alumina–13% Titania gives better sliding wear resistance than Alumina–3% Titania and Alumina 40% Titania composite coatings. The results show that the sliding wear rate decreases with increasing CPSP in both combination coatings. The Alumina–40% Titania coating gives very poor sliding wear resistance and its value also increases while increasing CPSP. Already the XRD results show the domination of rutile phase in Alumina–40% Titania which increases with increasing CPSP conditions rather than α- and γ-Al_2O_3. Generally the rutile phase gives poor anti wear properties compared to Alumina. In Alumina–13% Titania composite coating the rutile phase dominates, however α- and γ-Al_2O_3 phase also randomly appear. While increasing CPSP, the percentage of α-Al_2O_3 was increased and it gave better wear resistance. Fig. 15 shows the sliding wear rate of plasma sprayed Alumina–13% Titania composite coatings as a function of applied load. While increasing the load, consequently the wear loss also increases in all CPSP cases.

3.6. CSPS effect on erosive wear rate

Fig. 16 shows the erosive wear rate of plasma sprayed different compositions of Alumina–Titania composite coatings at different CPSP conditions. The erosive wear rate decreases with increase in CPSP for all compositions. Increase in CPSP gives better microstructure coating due to the higher degree of melting. The results show that the addition of TiO_2 increases the erosive wear rate. The maximum erosive rate was obtained at CPSP 833.33 in Alumina–40% Titania composite coating. The erosive wear of the coating mainly depends on the bonding

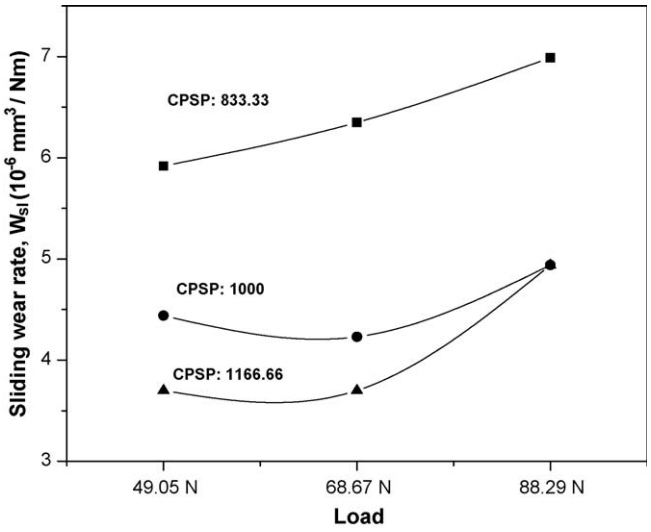

Fig. 15. Effect of applied load on the sliding wear rate of the plasma sprayed Alumina–13% Titania composite coatings at different CPSP.

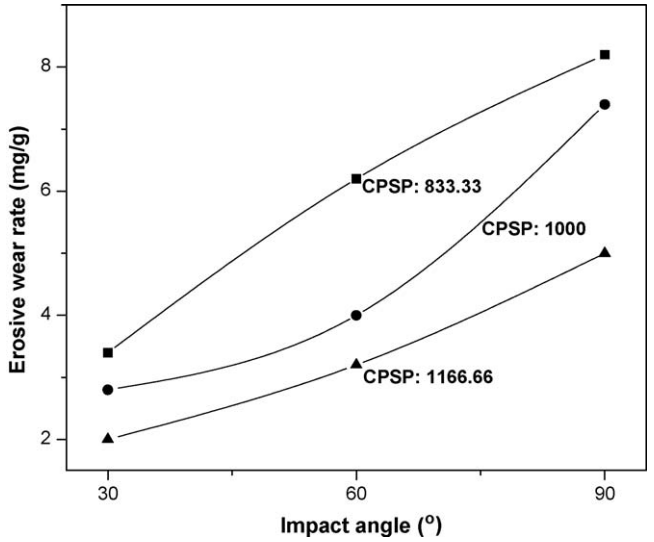

Fig. 17. Effect of impact angle on erosive wear rate of plasma sprayed Alumina + 13% Titania composite coating.

strength of the inter-lamella and surface smoothness of the coating materials.

Fig. 17 shows the influence of erodent impact angle on erosive wear rate of plasma sprayed Alumina–13% Titania at different CPSP conditions. Increasing impact angle increases the erosive wear of the coatings. In low impact angle (30°), the kinetic energy of the impinging particles contributes mainly to ploughing (horizontal component of the energy, proportional to cos(15°), ∼97%) and very little (normal component proportional to sin (15°), ∼3%) to normal repeated impact. Therefore insufficient energy does not initiating and propagating the grain boundary microcracks. But in 90° impact angle, majority of the kinetic energy is devoted to this process. As a result, the material removal rate at low impact angle is much lower than that at normal (90°) impact angle [23].

4. Conclusion

Atmospheric plasma sprayed Alumina–Titania composites coatings in different compositions (Alumina–3%, 13% and 40% Titania) were prepared for different CPSP conditions (833.33, 1000, 1166.66). At CPSP 1166.66, the Alumina–13% Titania composite coating gives best sliding wear resistance and lowest porosity. The Alumina–3% Titania composite coating gives best erosive wear resistance and highest microhardness values at CPSP 1166.66. At the same time the Alumina–40% Titania composite coating gives lowest microhardness and highest porosity at CPSP 1166.66.

Acknowledgements

The present study was supported by a grant from The Department of Science and Technology (DST), Government of India. Authors would like to thank Dr. P. Saravanan, DMRL, Hyderabad for their help in coating characterization. One of the authors (S.Y.) acknowledges the Junior Research Fellowship awarded by DST, Government of India.

References

[1] R.C. Tucker, Surface Engineering, ASM Metals Hand Book, ASM International, 1998.
[2] L. Pawlowski, The Science and Engineering of Thermal Spray Coatings, John Wiley & Sons, England, 1995.
[3] F. Ustel, S. Soykan, E. Celik, E. Avci, Plasma spray coating technology, J. Metall. 97 (1995) 31–37.
[4] E.H. Jordan, M. Gell, Y.H. Sohn, D. Goberman, L. Shaw, S. Jiang, M. Wang, T.D. Xiao, Y. Wang, P. Strutt, Fabrication and evaluation of plasma sprayed nanostructured Alumina–Titania coatings with superior properties, Mater. Sci. Eng. A301 (2001) 80–89.
[5] L. Shaw, D. Goberman, M. Gell, S. Jiang, Y. Wang, T.D. Xiao, P. Strutt, The dependency of microstructure and properties of nanostructured coatings on plasma spray conditions, Surf. Coat. Technol. 130 (2000) 1–8.
[6] R. Venkataraman, S. Pabla Singh, B. Venkataraman, D.K. Das, L.C. Pathak, S. Ghosh Chowdhury, R.N. Ghosh, D. Ravichandra, G.V. Narasima Rao, K. Nair, R. Kathirkar, A scanning electron microscopic study to observe the changes in the growth morphology of the α phased Alumina–13 wt.% titania coatings during plasma spraying, Surf. Coat. Technol. 202 (21) (2008) 5074–5083.
[7] H. Ageorges, P. Ctibor, Comparison of the structure and wear resistance of Al_2O_3–13 wt.%TiO_2 coatings made by GSP and WSP plasma process with two different powders, Surf. Coat. Technol. 202 (18) (2008) 4362–4368.
[8] P.V.A. Padmanabhan, Plasma Spraying: Principles and Applications, in: D.S. Patil, P.V.A. Padmanabhan, A.K. Das (Eds.), Proceeding of DAE-BRNS Workshop on Plasma Surface Engineering, BARC, Mumbai, India, (2005), pp. 254–264.
[9] A. Kucuk, R.S. Lima, C. Berndt, Influence of plasma spray parameters on formation and morphology of ZrO2–8 wt% Y2O3 deposits, J. Am. Ceram. Soc. 84 (4) (2001) 693–700.
[10] M. Bounazef, S. Guessasma, G. Montavon, C. Coddet, Effect of APS process parameters on wear behaviour of Alumina–Titania coatings, Mater. Lett. 58 (2004) 2451–2455.
[11] N.K. Joshi, S.N. Sahasrabudhe, K.P. Sreekumar, N. Venkatramani, Axial variation of electron density in thermal plasma spray jet, Eur. Phys. J. D 26 (2003) 215–219.
[12] S. Yugeswaran, V. Selvarajan, Electron number density measurement on a DC argon plasma jet by stark broadening of Ar I spectral line, Vacuum 81 (3) (2006) 347–352.
[13] W.L. Wise, J.W. Brault, K. Danzmann, V. Helbig, M. Kock, Unified set of atomic transition probabilities of neutral argon, Phys. Rev. A: Gen. Phys. 39 (1998) 2461–2471.
[14] S.A.R. Hashmi, U.K. Dwivedi, N. Chand, Graphite modified cotton fibre reinforced polyester composites under sliding wear conditions, Wear 262 (2007) 1426–1432.
[15] P. Saravanan, V. Selvarajan, S.V. Joshi, G. Sundararajan, Experimental design and performance analysis of alumina coatings deposited by detonation spray process, J. Phys. D: Appl. Phys. 34 (1) (2001) 131–140.
[16] J. Suchanek, P. Smrkovsky, N.A. Blaskovic, Grinberg, Erosive and hydroabrasive resistance of hardfacing materials, Wear 233–235 (1999) 229–236.
[17] G. Antou, G. Montavon, F. Hlawka, A. Cornet, C. Coddet, Characterization of the pore-crack network architecture of thermal-sprayed coatings, Mater. Charact. 53 (2004) 361–372.
[18] S. Kumar, V. Selvarajan, P.V.A. Padmanabhan, K.P. Sreekumar, Characterization and comparison between ball milled and plasma processed iron–aluminium thermal spray coatings, Surf. Coat. Technol. 201 (3–4) (2006) 1267–1275.
[19] S. Safai, H. Herman, Plasma Sprayed Materials, Treatise on Materials Science and Technology, vol. 20, Academic Press, New York, 1981.
[20] G. Barbezat, A.R. Nicoll, A. Sickinger, Abrasion, erosion and scuffing resistance of carbide and oxide ceramic thermal sprayed coatings for different applications, Wear 162 (1993) 529.
[21] M.K. Rerer (Ed.), Phase Diagrams for Ceramics, The American Ceramic Society, Inc., 1964.
[22] R. McPherson, The relationship between the mechanism of formation, microstructure and properties of plasma-sprayed coatings, Thin Solid Films 83 (1981) 297–310.
[23] Y. Zhang, Y.B. Cheng, S. Lathabai, Erosion of alumina ceramics by air- and water-suspended garnet particles, Wear 240 (2000) 40–51.
[24] V. Fervel, B. Normand, C. Coddet, Tribological behaviour of plasma sprayed Al_2O_3-based cermet coating, Wear 230 (1999) 70–77.
[25] B. Normand, V. Fervel, C. Coddet, V. Nikitine, Tribological properties of plasma sprayed Alumina–Titania coating: role and control of microstructure, Surf. Coat. Technol. 123 (2000) 278–287.
[26] D. Goberman, Y.H. Shon, L. Shaw, E. Jordan, M. Gell, Microstructure development of Al_2O_3–13 wt.% TiO_2 plasma sprayed coating derived from nonocrystalline powders, Acta Mater. 50 (2002) 1141–1152.